Crystal-field ground state of the noncentrosymmetric superconductor CePt₃Si: A combined polarized soft x-ray absorption and polarized neutron study

T. Willers,[1] B. Fåk,[2] N. Hollmann,[1] P. O. Körner,[1] Z. Hu,[1] A. Tanaka,[3] D. Schmitz,[4] M. Enderle,[5] G. Lapertot,[2] L. H. Tjeng,[1] and A. Severing[1]

[1]*Institute of Physics II, University of Cologne, Zülpicher Straße 77, D-50937 Cologne, Germany*
[2]*Commissariat à l'Energie Atomique, INAC, SPSMS, 38054 Grenoble, France*
[3]*Department of Quantum Matter, ADSM, Hiroshima University, Higashi-Hiroshima 739-8530, Japan*
[4]*Helmholtz-Zentrum Berlin, BESSY II, Albert-Einstein-Straße 15, D-12489 Berlin, Germany*
[5]*Institut Laue Langevin, 6 rue Horowitz, 38042 Grenoble, France*

We determined the crystal-field split Hund's rule ground state of the noncentrosymmetric heavy fermion superconductor CePt₃Si with polarization dependent soft x-ray absorption spectroscopy (XAS) and polarized neutron scattering. We are also able to give the sequence of the crystal-field states from the temperature evolution of the linear dichroic signal in the XAS. The quantitative analysis of the XAS temperature dependence together with the neutron transition energies complete the identification of the crystal-field level scheme.

I. INTRODUCTION

The discovery of superconductivity in the antiferromagnetic phases of the noncentrosymmetric heavy fermion compounds CePt₃Si,[1] CeIrSi₃,[2] and CeRhSi₃[3] stimulated a flurry of theoretical and experimental activities[4–7] with the main interest to understand the pairing state in the absence of inversion symmetry. It seems that the superconductivity is due to a mixture of singlet and triplet Cooper pairing and that the superconducting state is magnetically driven.[8,9] The unusual properties evolve from the hybridized 4f electrons so that the question of which influence the highly anisotropic crystal-field ground state may have on the hybridization between 4f and conduction electrons arises. Attempts were made to investigate this issue for the heavy fermion compound CeRu₂Si₂,[10] and the semiconducting Kondo materials CeNiSn (Refs. 11 and 12) and CeRhAs.[13] More recently the aspect of q-dependent hybridization was also studied in the CeMIn₅ compounds.[14–17] However, reliable experimental input for such theoretical investigation is scarce due to experimental uncertainties in determining the 4f ground-state wave functions.

The wave functions and crystal-field levels are usually determined from a combined analysis of single-crystal susceptibility and polycrystalline neutron-scattering measurements. However, the method often fails because of thermal or powder averaging in either technique, and additionally, neutron scattering suffers from phonon contributions and broadened crystal-field levels due to hybridization effects.[18] Moreover, in the presence of magnetic order, anisotropic molecular-field parameters have to be introduced in order to fit the static susceptibility, ending up with too many free parameters for a unique description. The methods to apply are then inelastic or elastic polarized neutron scattering on single crystals, the first technique requiring large single crystals, the second being very sensitive to absorption corrections when determining the 4f magnetic form factor.

We have shown for the case of the heavy fermion material CePd₂Si₂ that soft x-ray absorption at the Ce M₄,₅ edges can be used complementary to neutron scattering in order to de-termine the ground-state wave function.[19] X-ray absorption spectroscopy (XAS) is highly sensitive to the initial state and via its polarization dependence direct information about the $|J_z\rangle$ admixtures of the ground-state wave function can be obtained. Sensitivity for higher lying crystal-field states is achieved by thermally populating those states. It was shown in Ref. 19 that the capability of XAS to resolve closely lying crystal-field states is not determined by the energy resolution of the experimental setup, but rather by the temperature. However, the exact energy of crystal-field excitations is most accurately determined with inelastic polarized neutron scattering on single crystals where phonon and magnetic scattering can be separated. Hence it is ideal to combine both techniques.

CePt₃Si orders antiferromagnetically at T_N=2.2 K and enters a superconducting state at $T_{sc} \approx 0.75$ K.[1] The coexistence of both states has been confirmed by several experimental techniques.[20,21] The low-energy magnetic excitations were recently measured on a single crystal using inelastic neutron scattering.[22] CePt₃Si crystallizes in the noncentrosymmetric tetragonal space group $P4mm$ with lattice constants a=4.072 Å and c=5.442 Å.[23] Inversion symmetry is broken by the absence of a mirror plane perpendicular to the c axis. However, the lack of inversion symmetry is irrelevant for the crystal-field description since the 4f wave functions are even functions. Therefore, as in other centrosymmetric compounds, the Hund's rule ground state of Ce³⁺ (J=5/2, point group $C_{4v} \in D_{4h}$) (Ref. 24) splits under the influence of a tetragonal crystal field, into three Kramer's doublets, which can be represented in the basis of $|J_z\rangle$. The eigenfunctions of the three Kramer's doublets can be written as

$$|2\rangle = |\pm 1/2\rangle,$$

$$|1\rangle = \beta|\pm 5/2\rangle - \alpha|\mp 3/2\rangle,$$

$$|0\rangle = \alpha|\pm 5/2\rangle + \beta|\mp 3/2\rangle, \quad (1)$$

with $\alpha^2 + \beta^2 = 1$ and an arbitrarily chosen phase of the mixed states.

Two groups have published inelastic neutron-scattering data of CePt$_3$Si powder samples in order to determine the crystal-field scheme. Bauer *et al.*[25] found a broad distribution of magnetic intensity between 10 and 30 meV, which was fitted with two nonresolved crystal-field excitations centered at 13 and 20 meV. The crystal-field parameters of Bauer *et al.* yield $|0\rangle = 0.59|\pm 5/2\rangle + 0.81|\mp 3/2\rangle$ for the ground-state wave function and $|2\rangle = |\pm 1/2\rangle$ as the highest excited state at 20 meV. This crystal-field scenario is supported by specific-heat data on La doped CePt$_3$Si.[26] Metoki *et al.*[27] found also a mixed ground state, but interpreted their neutron data with a very different ground state mixing of $|0\rangle = 0.93|\pm 5/2\rangle + 0.37|\mp 3/2\rangle$. According to their data the $|\pm 1/2\rangle$ state is 1 meV above the ground state and the second mixed state is at 24 meV. The latter crystal-field energies seem in agreement with specific-heat and susceptibility data by Takeuchi *et al.*[28]

In this paper, we determine the ground-state wave function from the low-temperature XAS data, i.e., the value of the mixing factor α, which gives the actual spatial distribution of the crystal-field ground state. We will further show that the temperature dependence of the XAS data determines the sequence of states. A quantitative modeling of the temperature dependence can even be done provided that the crystal-field energies are known. The latter are determined from the polarized inelastic neutron data presented here. Thus a complete picture of the crystal-field level scheme has been achieved.

II. EXPERIMENT

The CePt$_3$Si single crystal used for this study was the same as in Ref. 22. A thin slice was cut from this crystal and used for the XAS measurements. We recorded all spectra using the total electron yield method in a chamber with a pressure of 4×10^{-11} mbar at the UE-46 PGM-1 undulator beam line of BESSY II. The total electron yield signal was normalized to the incoming photon flux I_0 as measured at the refocusing mirror. Clean sample surfaces were obtained by cleaving the samples *in situ*. The energy resolution at the cerium $M_{4,5}$ edges ($h\nu \approx 875 - 910$ eV) was set at 0.15 eV. Further, the undulator together with a normal incident measurement geometry allows for a change of polarization without changing the probed spot on the sample surface. This guarantees a reliable comparison of the spectral line shapes. The two polarizations were $E \perp c$ and $E \parallel c$, c being the long tetragonal axis. The sample was cleaved and then cooled down to the lowest accessible temperature. Spectra were taken at 5, 50, 150, and 200 K while warming up. In order to assure reproducibility of the data the sample was cleaved a second time and then data were taken in the sequence 300, 50, and 80 K.

Inelastic neutron-scattering measurements using polarization analysis were performed on the thermal triple-axis spectrometer IN20 at the high-flux reactor of the Institut Laue Langevin. Horizontally focusing Heusler monochromator and analyzer were used in combination with relaxed collimation and a fixed final energy of 14.7 meV with an energy resolution [full width at half maximum (FWHM)] of 0.6 meV. Higher-order neutrons were removed from the scat-

tered beam using a graphite filter and their contribution to the monitor count rate was corrected for. Measurements were performed in the paramagnetic phase at a temperature of 5 K with the wave-vector transfer **Q** either parallel to the *a* or to the *c* axis, but with the same value of $Q = |\mathbf{Q}|$, to eliminate the influence of the magnetic form factor to the measured intensities. The use of polarization analysis in combination with a single crystal has two advantages for crystal-field determinations compared with standard methods of unpolarized neutrons on a polycrystalline material: (i) Scattering from phonons can easily be subtracted; (ii) Separating the $j = x, y, z$ components of the angular-momentum operator M_j, where M_j is the operator of the transition matrix elements $|M_j^\perp|^2 \equiv |\langle f|M_j^\perp|i\rangle|^2$ between the initial state i and the final state f. $\perp$ reflects the fact that only components perpendicular to **Q** are observed in neutron-scattering experiments.

We measured the three polarization components $\gamma = (\xi, \eta, \zeta)$ of the spin-flip cross section σ_γ, where ξ is parallel to **Q**, η is perpendicular to **Q** in the horizontal scattering plane, and ζ is vertical. The pure magnetic scattering is given by the difference of the spin-flip cross sections $\parallel$**Q** and $\perp$**Q** or, more specifically for the present setup, the different transition matrix elements of the M_j operator are given by $|M_z|^2 = \sigma_\xi - \sigma_\eta$ for **Q**$\parallel$**a** and $|M_x|^2 = |M_y|^2 = \sigma_\xi - \sigma_\zeta$ for **Q**$\parallel$**a** or $|M_x|^2 = |M_y|^2 = \sigma_\xi - \sigma_\eta = \sigma_\xi - \sigma_\zeta$ for **Q**$\parallel$**c**. The three independent determinations of $|M_x|^2$ are identical within statistical uncertainty. The measured non-spin-flip cross section shows no strong intensity that could leak through to the spin-flip channels via the finite flipping ratio of 20–23, which corresponds to a neutron polarization efficiency of 95% at both polarizer and analyzer.

III. RESULTS AND DISCUSSION

For the C_{4v} point symmetry the crystal-field Hamiltonian $H_{CF} = B_2^0 O_2^0 + B_4^0 O_4^0 + B_4^4 O_4^4$ describes the crystal-field potential when the three Stevens parameters B_2^0, B_4^0, and B_4^4 are determined. Alternatively the crystal-field potential can be expressed in terms of the transition energies E_1 and E_2 between the crystal-field states within the multiplet and the mixing parameter α. We performed ionic full multiplet calculations using the XTLS 8.3 program[29] to calculate the XAS spectra. All atomic parameters were given by Hartree-Fock values, with a reduction of about 35% for the 4f-4f Coulomb interactions and about 20% for the 3d-4f interactions to reproduce best the experimental isotropic spectra, $I_{iso} = 2I_\perp + I_\parallel$. These values compare well with our findings for other heavy fermion compounds[19] and account for the configuration-interaction effects not included in the Hartree-Fock scheme.

Once the atomic parameters are fine tuned to the isotropic spectra, the polarized XAS data can be described by the incoherent sums of the respective polarization-dependent spectra of the pure $|J_z\rangle$ states[19] as long as the crystal-field splitting is small with respect to the spin-orbit splitting. The latter requirement, which is fulfilled here ($E_{SO} \approx 280$ meV and $E_{CF} \leq 20$ meV), assures that interference terms resulting from intermixing between the $J = 5/2$ and $J = 7/2$ multiplet can be neglected.
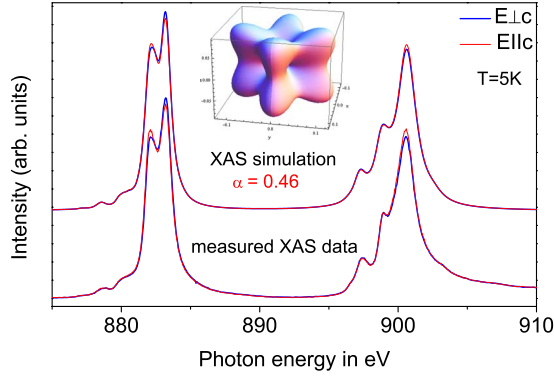
FIG. 1. (Color online) Measured and simulated linear polarized XAS spectra of CePt$_3$Si at the $M_{4,5}$ edges at $T=5$ K. The inset shows the corresponding spatial distribution.

FIG. 2. (Color online) Simulated polarizations for pure $|J_z\rangle$ states of Ce^{3+} and sum of the three polarization dependent $|J_z\rangle$ spectra. The insets resemble the spatial distributions.

Figure 1 shows the low-temperature linear polarized XAS data of CePt$_3$Si at the $M_{4,5}$ edge and their simulation based on the full multiplet treatment as described above. The polarization dependence is small. It certainly does not match that of a pure $|\pm 1/2\rangle$ state as can be seen from Fig. 2, where we have shown again (see Ref. 19) for reasons of convenience the polarization dependent spectra for each $|J_z\rangle$ state. It also does not match that of a pure $|\pm 3/2\rangle$ nor $|\pm 5/2\rangle$ state so that the solution obeying the tetragonal crystal-field symmetry should be sought in a mix of these two. We found that the 5 K data are best described by the ground state

$$|0\rangle = 0.46|\pm 5/2\rangle + 0.89|\mp 3/2\rangle$$

($\alpha=0.46\pm 0.03$) without the necessity to include the fractional occupation of a higher lying state. The small size of
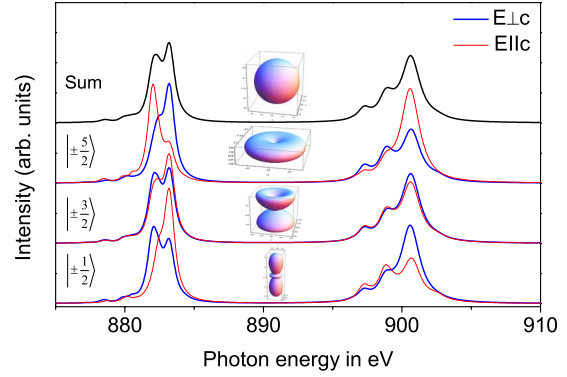
the polarization effect can be understood when considering, as was shown in the paper by Hansmann *et al.*,[19] that the variation in α from 0 to 1 leads to a vanishing polarization effect when α is equal to $\sqrt{1/6}=0.41$, i.e., when α is equal to the value of a cubic crystal-field symmetry. According to our data the mixing factor in CePt$_3$Si is close to this value.

In order to rule out that the small size of the effect in CePt$_3$Si is due to unwanted surface effects the sample was measured at several temperatures, cleaved a second time, and remeasured. The left panel side of Fig. 3 shows the M_5 edge of CePt$_3$Si for several temperatures between 5 and 300 K. After the first cleave data were taken at 5, 50, 150, and 200 K. After the second cleave the sample was measured first at 300 K and then cooled down to 50 K and warmed up to 80 K. Comparing the data at different temperatures shows that
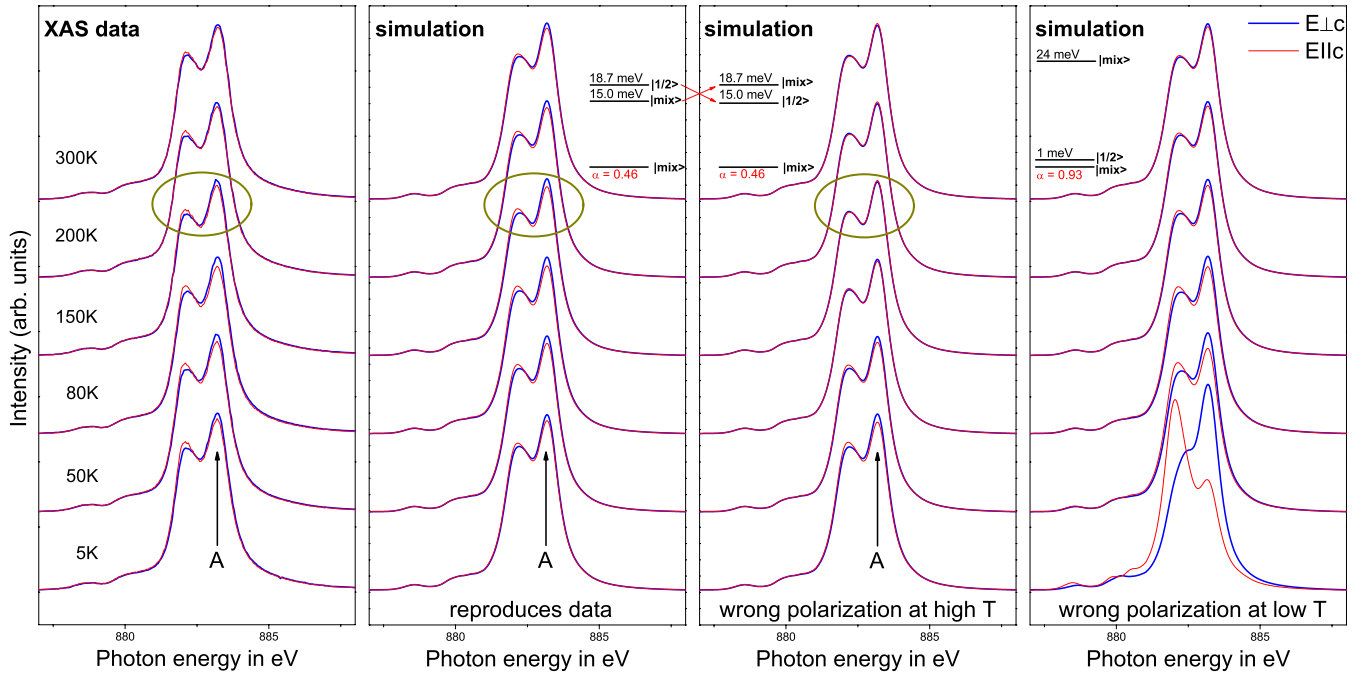

FIG. 3. (Color online) Left panel: temperature-dependent XAS data at the M_5 edge. Two middle panels: simulation of spectra with ground-state wave function as determined from the 5 K XAS data and with crystal-field energies obtained from the polarized neutron data. The simulations in the middle columns have different sequences of states. Right panel: simulation with ground-state wave function and energies as given by Metoki *et al.* (Ref. 27).
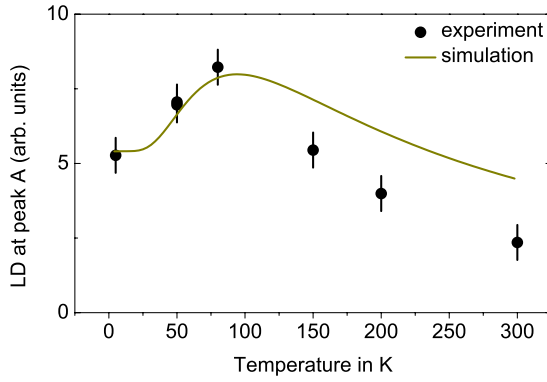
FIG. 4. (Color online) Difference of the intensities $E \perp c$ and $E \| c$ [*linear dichroism* (LD)] at peak A of the M_5 edge versus temperature. The black dots are determined from the experimental data (left panel in Fig. 3), the dark yellow line results from a simulation according to the left, middle panel in Fig. 3.

the polarization increases from 5 to 50 K and 80 K and then decreases again as temperature rises further. We conclude that this effect is real since the polarization at 300 K (measured first after second cleave) is smaller than the polarization at 50 K (measured second after second cleave) and 80 K (measured third after second cleave). Surely, if surface degradation with time had been present, then one would rather expect to see a decrease in polarization. In addition the 50 K data were well reproduced. The black dots in Fig. 4 are the difference of the two intensities $E \perp c$ and $E \| c$ [called *linear dichroism* (LD)] at the high energy peak A of the M_5 edge (see Fig. 3) and they summarize the temperature evolution of the polarization effect.

Polarized inelastic neutron scattering was used to determine the energy of the crystal-field levels. Figure 5 shows energy scans for $\mathbf{Q} = (1.5, 0, 0)$ for different cross sections sensitive to M_x and M_z, respectively. Within the crystal-field
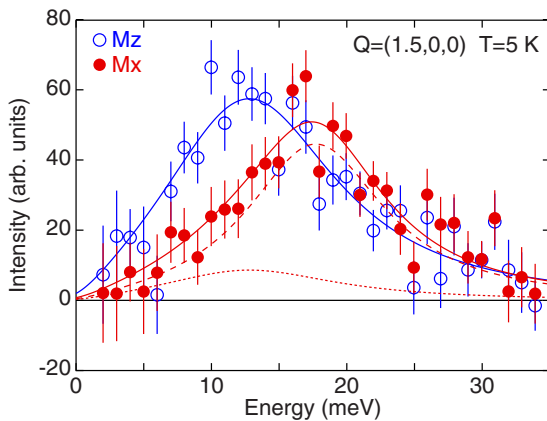

FIG. 5. (Color online) Magnetic intensities as obtained from neutron-scattering difference spectra taken at $\mathbf{Q} = (1.5, 0, 0)$ and $T = 5$ K. Open blue symbols and line: experimental data of the $|M_z|^2$ component and fit to the transition $|0\rangle \rightarrow |1\rangle$. Full red symbols: experimental data of the $|M_x|^2$ component, which includes the transition $|0\rangle \rightarrow |1\rangle$ (dotted red line, all parameters fixed, see text) as well as the transition $|0\rangle \rightarrow |2\rangle$ (dashed red line, all parameters free). The full red line is the sum of both contributions.

scheme of Eq. (1), the M_z cross section (open blue symbols in Fig. 5) contributes only to the transition between the ground state $|0\rangle$ and the first-excited state $|1\rangle$. The data were fitted by a damped harmonic oscillator (DHO) (Ref. 30) convoluted with the instrumental resolution function. The first-excited state $|1\rangle$ has an energy (with respect to the ground-state energy) of $E_1 = 15.0(4)$ meV and a width [half width at half maximum (HWHM)] of 8.2(9) meV, which reflects the damping of the crystal-field excitation due to the hybridization with the conduction electrons. Because of the strong damping the excitation energy of the DHO varies from the peak maximum. The M_x cross section contains both transitions, $|0\rangle \rightarrow |1\rangle$ and $|0\rangle \rightarrow |2\rangle$, and the corresponding data (full red symbols in Fig. 5) were modeled with two DHOs. The energy and width of the first transition ($|0\rangle \rightarrow |1\rangle$) in the M_x data were kept fixed to the above M_z values, while the M_x intensity of this transition was calculated from scaling the transition probabilities according to the XAS ground-state wave function. The second DHO describes the second transition ($|0\rangle \rightarrow |2\rangle$) and here position, width, and intensity were fitted. The best fit yields $E_2 = 18.7(5)$ meV and HWHM $= 6.2(8)$ meV. The fitted integrated intensity of the second transition is about 16% smaller than expected from a scaling with the XAS ground-state wave function. We consider this to be an excellent agreement between neutron intensities and our findings from XAS.

The temperature dependence of the XAS data can now be modeled quantitatively using the ground-state wave function as determined from XAS at $T = 5$ K and the energy levels as determined with polarized neutrons. The results of these calculations are shown in the two middle panels of Fig. 3. The simulations differ in the order of the first- and second-excited state. Only the simulation with the $|\pm 1/2\rangle$ as highest state reproduces the temperature dependence of the data well. The other option with the $|\pm 1/2\rangle$ as first-excited state leads to an inversion of polarization as temperature rises: for example, the intensity of peak A for $E \perp c$ (blue) is simulated to become smaller than for $E \| c$ (red) at 150 K, in contradiction with the experiment, see dark yellow circles in the left and middle right panel of Fig. 3. This can be understood when looking at the pure states as displayed in Fig. 2 and keeping in mind that the XAS spectra at finite temperatures resemble the superimposed polarizations of each state. The top of Fig. 2 shows that the full thermal population of all crystal-field states leads to a vanishing polarization since the sum of all $|J_z\rangle$ spatial distributions is spherical. From this it can be concluded that a small ground-state polarization requires the first- and second-excited state to almost compensate each other, i.e., the other mixed state must have a polarization almost opposite to the one of the $|\pm 1/2\rangle$ (see Fig. 2). Hence mixing in the other mixed state as temperature rises leads at first to an increase in polarization until the influence of the highest state, here the $|\pm 1/2\rangle$, compensates this due to thermal population. The dark yellow line in Fig. 4 displays the simulated temperature dependence of the polarization. The simulation reproduces the experimental temperature dependence quite well, including the presence of a maximum at 80 K. The Stevens parameters which give the right energies, wave functions, and sequence of states are $B_2^0 = -0.224$ meV, $B_4^0 = 0.047$ meV, and $|B_4^4| = 0.228$ meV.

For completeness we have simulated the XAS spectra using the crystal-field model suggested by Metoki *et al.*[27] Their ground-state wave function produces spectra which do not resemble the experimental ones (see right panel of Fig. 3). Moreover, their model would lead to a strong temperature dependence between 5 and 50 K, which is not present in the experimental data.

IV. CONCLUSION

We have performed temperature-dependent linear polarized XAS measurements at the $M_{4,5}$ edge of cerium in CePt$_3$Si and inelastic polarized neutron experiments. The combination of both techniques gives a conclusive picture of the crystal-field level scheme in CePt$_3$Si. The low-temperature XAS data yield $0.46|\pm 5/2\rangle + 0.89|\mp 3/2\rangle$ as the ground-state wave function and the sequence of excited states can clearly be determined from the temperature dependence of the XAS data. Using the crystal-field transition energies as determined from the polarized neutron-scattering data (15.0 and 18.7 meV), we were also able to quantitatively explain the temperature dependence. The wave-vector and polarization dependences of the neutron-scattering intensities also confirm this sequence of the crystal-field levels. We note that the result with having the $|\pm 1/2\rangle$ level as the highest lying excited state is in excellent agreement with the findings by Bauer *et al.* and excludes the suggestions by Metoki at al.

[1] E. Bauer, G. Hilscher, H. Michor, Ch. Paul, E. W. Scheidt, A. Gribanov, Yu. Seropegin, H. Noël, M. Sigrist, and P. Rogl, Phys. Rev. Lett. **92**, 027003 (2004).

[2] I. Sugitani, Y. Okuda, H. Shishido, T. Yamada, A. Thamizhavel, E. Yamamoto, T. D. Matsuda, Y. Haga, T. Takeuchi, R. Settai, and Y. Onuki, J. Phys. Soc. Jpn. **75**, 043703 (2006).

[3] N. Kimura, K. Ito, K. Saitoh, Y. Umeda, H. Aoki, and T. Terashima, Phys. Rev. Lett. **95**, 247004 (2005).

[4] E. Bauer, H. Kaldarar, A. Prokofiev, E. Royanian, A. Amato, J. Sereni, W. Brämer-Escamilla, and I. Bonalde, J. Phys. Soc. Jpn. **76**, 051009 (2007).

[5] S. Fujimoto, J. Phys. Soc. Jpn. **76**, 051008 (2007).

[6] N. D. Mathur, F. M. Grosche, S. R. Julian, I. R. Walker, D. M. Freye, R. K. W. Haselwimmer, and G. G. Lonzarich, Nature (London) **394**, 39 (1998).

[7] K. V. Samokhin, E. S. Zijlstra, and S. K. Bose, Phys. Rev. B **69**, 094514 (2004).

[8] L. P. Gor'kov and E. I. Rashba, Phys. Rev. Lett. **87**, 037004 (2001).

[9] S. S. Saxena and P. Monthoux, Nature (London) **427**, 799 (2004).

[10] G. Zwicknagl, Adv. Phys. **41**, 203 (1992).

[11] H. Ikeda and K. Miyake, J. Phys. Soc. Jpn. **65**, 1769 (1996).

[12] Y. Kagan, K. A. Kikoin, and A. S. Mishchenko, Phys. Rev. B **55**, 12348 (1997).

[13] F. Ishii and T. Oguchi, J. Phys. Soc. Jpn. **73**, 145 (2004).

[14] F. P. Mena, D. van der Marel, and J. L. Sarrao, Phys. Rev. B **72**, 045119 (2005).

[15] K. S. Burch, S. V. Dordevic, F. P. Mena, A. B. Kuzmenko, D. van der Marel, J. L. Sarrao, J. R. Jeffries, E. D. Bauer, M. B. Maple, and D. N. Basov, Phys. Rev. B **75**, 054523 (2007).

[16] P. Ghaemi and T. Senthil, Phys. Rev. B **75**, 144412 (2007).

[17] H. Weber and M. Vojta, Phys. Rev. B **77**, 125118 (2008).

[18] J.-G. Park, D. T. Adroja, K. A. McEwen, Y. J. Bi, and J. Kulda, Phys. Rev. B **58**, 3167 (1998).

[19] P. Hansmann, A. Severing, Z. Hu, M. W. Haverkort, C. F. Chang, S. Klein, A. Tanaka, H. H. Hsieh, H.-J. Lin, C. T. Chen, B. Fåk, P. Lejay, and L. H. Tjeng, Phys. Rev. Lett. **100**, 066405 (2008).

[20] M. Yogi, Y. Kitaoka, S. Hashimoto, T. Yasuda, R. Settai, T. D. Matsuda, Y. Haga, Y. Onuki, P. Rogl, and E. Bauer, Phys. Rev. Lett. **93**, 027003 (2004).

[21] A. Amato, E. Bauer, and C. Baines, Phys. Rev. B **71**, 092501 (2005).

[22] B. Fåk, S. Raymond, D. Braithwaite, G. Lapertot, and J.-M. Mignot, Phys. Rev. B **78**, 184518 (2008).

[23] A. I. Tursina, A. V. Gribanov, H. Noel, P. Rogl, Y. D. Seropegin, and O. I. Bodak, J. Alloys Compd. **383**, 239 (2004).

[24] P. A. Frigeri, D. F. Agterberg, A. Koga, and M. Sigrist, Phys. Rev. Lett. **92**, 097001 (2004).

[25] E. Bauer, G. Hilscher, H. Michor, M. Sieberer, E. W. Scheidt, A. Gribanov, Yu. Seropegin, P. Rogl, A. Amato, W. Y. Song, J.-G. Park, D. T. Adroja, M. Nicklas, G. Sparn, M. Yogi, and Y. Kitaoka, Physica B **359-361**, 360 (2005).

[26] St. Laumann, R. Lackner, H. Michor, G. Hilscher, and E. Bauer, Physica B **378-380**, 386 (2006).

[27] N. Metoki, K. Kaneko, T. D. Matsuda, A. Galatanu, T. Takeuchi, S. Hashimoto, T. Ueda, R. Settai, Y. Onuki, and N. Bernhoeft, J. Phys.: Condens. Matter **16**, L207 (2004).

[28] T. Takeuchi, S. Hashimoto, T. Yasuda, H. Shishido, T. Ueda, M. Yamada, Y. Obiraki, M. Shiimoto, H. Kohara, T. Yamamoto, K. Sugiyama, K. Kindo, T. D. Matsuda, Y. Haga, Y. Aoki, H. Sato, R. Settai, and Y. Onuki, J. Phys.: Condens. Matter **16**, L333 (2004).

[29] A. Tanaka and T. Jo, J. Phys. Soc. Jpn. **63**, 2788 (1994).

[30] B. Fåk and B. Dorner, Physica B **234-236**, 1107 (1997).